UDC: 542.8+544.6 doi: 10.33609/2708-129X.92.5.2026.19-30

INFLUENCE OF THE NATURE OF A BINDER ON THE ELECTROCHEMICAL PROPERTIES OF THE $LiMn_{0.7}Fe_{0.3}PO_4$ CATHODE MATERIAL

O.V. Potapenko[1] https://orcid.org/0000-0002-0169-2403
H.V. Potapenko[1,2] https://orcid.org/0000-0002-1071-0183
V.O. Oliinyk[1] https://orcid.org/0000-0002-0929-8662
V.A. Sirosh[1] https://orcid.org/0000-0001-9620-8073
Changji Zhou[2] https://orcid.org/0009-0006-2539-0692
Chee Sien Wong [2,3] https://orcid.org/0000-0003-4504-3664
Changbo Yu[2] https://orcid.org/0009-0001-1912-9766
Chenchun Zhang[2] https://orcid.org/0009-0009-2203-0503

[1]V.I. Vernadsky Institute of General and Inorganic Chemistry of the National Academy of Sciences of Ukraine, 32/34 Acad. Palladina Ave., 03142 Kyiv, Ukraine;
[2]Zhejiang Casnovo New Materials Co., Ltd., No.1 Zhongke Road, Zhanmao Street, Putuo District, Zhoushan City, Zhejiang Province, China;
[3]School of Petrochemical Engineering and Environment, Zhejiang Ocean University, No. 1, Haida South Road, Lincheng Street, Dinghai District, Zhoushan City, Zhejiang Province, China
**e-mail: 1978hiking@gmail.com*

This study presents an electrochemical comparison of $Li||LiMn_{0.7}Fe_{0.3}PO_4$ coin cells using two different polymers as binders: PVDF and the water-soluble binder NV-1A. The charge/discharge curves obtained at a current rate of 0.05 C exhibit two well-defined plateaus at approximately 3.5 V and 4.1 V, corresponding to the Fe^{2+}/Fe^{3+} and Mn^{2+}/Mn^{3+} redox pairs, respectively. The capacity ratio of these plateaus is about 7:3, which matches the Mn/Fe ratio in the pristine material. The specific capacity of the coin cells with different binders falls within the range of 137–141 $mAh \cdot g^{-1}$, which is consistent with the manufacturer's specifications for the material. However, upon the first cycles, the coin cells with NV-1A binder exhibit a slightly lower specific capacity. This is attributed to the possible formation of Li_3PO_4 particles on the electrode surface, which leads to a decrease in specific capacity upon the initial cycles but improves the overall stability upon prolonged cycling. The first-cycle coulombic efficiency is 96.0 % for PVDF and 94% for NV-1A, increasing to 99.5% ± 0.1 % upon further cycling for both systems. Increasing the charge/discharge current density leads to a decrease in the specific capacity of $Li||LiMn_{0.7}Fe_{0.3}PO_4$ electrodes. This decrease is more pronounced for PVDF. At 0.5 C, the specific capacity reaches 68 $mAh \cdot g^{-1}$ for PVDF and 85 $mAh \cdot g^{-1}$ for NV-1A. Cyclic stability tests reveal that, despite the lower initial capacity of the NV-1A based coin cells, their capacity fade rate is only 0.1 % per cycle at 0.1 C, compared with 0.45 % for PVDF. Consequently, after 75 cycles, the NV-1A coin cells exhibit superior capacity retention. These findings are further discussed in the context of electrode degradation mechanisms upon cycling.

Key words: polymer binder, water-soluble binder, lithium manganese ion phosphate, galvanoatatic cycling, electrochemical impedance spectroscopy, capacity retention.

INTRODUCTION.

The development of lithium-ion battery (LIB) technologies is one of the key directions of modern science [1], driven by their widespread application in electric vehicles, energy storage systems, and portable electronic devices [2]. Particular attention has been paid to olivine-structured cathode materials [3, 4], especially $LiMn_xFe_{1-x}PO_4$ (LMFP) [5], which combines the high thermal stability of $LiFePO_4$ (LFP) with the elevated operating voltage (~4.1 V) characteristic of $LiMnPO_4$ [6, 7]. As a result, LMFP provides a higher energy density compared to conventional LFP (~3.4 V) without a significant loss of safety [8, 9]. However, LMFP exhibits intrinsically low electronic conductivity ($\approx 10^{-10}$–10^{-9} S/cm) and slow lithium-ion diffusion kinetics, which adversely affect its rate capability and cycling stability [6, 9].

One of the effective approaches to improving the electrochemical parameters of $LiMn_xFe_{1-x}PO_4$ is the optimization of electrode composition, particularly through the selection of a suitable polymer binder. As an essential component of LIB electrodes, the polymer binder mechanically holds together the active material particles and conductive additives, ensures adhesion to the current collector, and, via electrolyte wetting, facilitates lithium-ion transport to the cathode material. Improvement of the adhesive and cohesive properties of the binder positively affects the formation of the solid electrolyte interphase (SEI) during the initial charge–discharge cycles, which largely determines the overall resistance of both the electrode and the battery.

Polyvinylidene fluoride (PVDF) is traditionally used as a cathode binder; however, its processing requires the toxic organic solvent N-methyl-2-pyrrolidone (NMP). This complicates manufacturing, increases production costs, and raises environmental issues [10–12]. In recent years, the global trend has been towards replacing PVDF with water-soluble binders that are more cost-effective and environmentally friendly. Among them, polyacrylic acid (PAA)-based materials and their derivatives have attracted considerable interest [10–12], as they can reduce the internal resistance of electrode composites. Nevertheless, the rigid structure of PAA may lead to cracking of the electrode layer during cycling due to volume changes in the crystal lattice, resulting in the loss of electrical contact between particles and delamination of the electrode coating from the current collector.

To overcome these limitations, PAA is often modified with various monomers, particularly nitrogen-containing compounds, which improve adhesion through the formation of covalent bonds at the polymer–substrate interface [13] and enhance the flexibility of the material [14–17]. One such binder is NV-1A, a commercial water-soluble polymer based on polyacrylic acid modified with various monomers, including nitrogen-containing species, to improve its adhesive, cohesive, and mechanical properties.

Despite the considerable number of studies devoted to the synthesis and electrochemical performance of LMFP, the influence of polymer binders on the structural and electrochemical characteristics of LMFP cathodes remains insufficiently explored. Most recent investigations have focused on anode materials, whereas issues related to cathode microstructure formation, cycling stability, and adhesion properties remain largely unresolved [11, 18].

The aim of this work is to investigate the effect of binder type on the electrochemical

properties of $LiMn_{0.7}Fe_{0.3}PO_4$ cathode material. The combination of lithium manganese iron phosphate (LMFP) cathode material with a water-based polyacrylic acid (PAA) binder is a significant advancement in lithium-ion battery technology, offering novelty in i) environmental sustainability and manufacturing safety; (ii) superior electrochemical performance (PAA binders exhibit exceptional electrochemical properties that address key limitations of conventional binder systems); (iii) addressing LMFP-specific challenges (LMFP is a promising high-energy-density cathode material, but it suffers from manganese dissolution during charge-discharge cycles, which degrades battery life and storage performance. The novelty of PAA-based aqueous binders lies in their ability to mitigate this issue); (iv) superior adhesion and mechanical properties (the carboxyl-rich structure of PAA enables strong hydrogen bonding and covalent interactions with active material surfaces, providing excellent adhesion that maintains electrode integrity during volume changes. This is particularly valuable for LMFP cathodes, where structural stability is critical for long-term performance. Unlike conventional binders that rely on weak van der Waals forces, PAA offers robust mechanical properties essential for high-voltage operation); (v) cost-effectiveness and process compatibility (water-based PAA binders offer lower material costs and simplified manufacturing processes compared to NMP-based systems).

Thus, taking into account the above, the purpose of this work was to perform a comparative analysis of cycling performance and electrochemical impedance spectroscopy (EIS) data with two different binders. Based on the obtained results, the advantages of use the water-soluble NV-1A binder were evaluated, and possible explanations for the observed structural changes in the electrode material were proposed.

EXPERIMENT AND DISCUSSION OF THE RESULTS.

Commercial $LiMn_{0.7}Fe_{0.3}PO_4$ sample ("Qiquling Electrochemistry", Guangzhou, China) has been used as the cathode material.

Electrochemical tests have been performed in sample $Li||LiMn_{0.7}Fe_{0.3}PO_4$ cells on a Neware potentiostat/galvanostat (Shenzhen, Guandong, China). Working electrodes have consisted of 90 wt. % of the studied material, 5 wt. % of a conductive additive (soot) and 5 wt. % of binders (poly (vinyliden) difluoride and NV-1A ("Zhejiang Casnovo New Materials Co Ltd.")). A 50 μm layer of the slurry was applied onto aluminum foil with a doctor blade and then dried at 100–120 °C 18-21 h under a vacuum. The mass loading of $LiMn_{0.7}Fe_{0.3}PO_4$ in a dried electrode was 6.5–9 $mg{\cdot}cm^{-2}$. To increase the cathode density and improve the electrical contact between the active material particles and the conductive additive, the electrodes were pressed at a pressure of 190 MPa. This process reduced the electrode thickness from 65–66 to 50–52 μm. Coin cells were assembled in 2032 cases with Celgard 2500 separators and an electrolyte containing the 1 M solution of $LiPF_6$ in a mixture of ethylene carbonate and dimethyl carbonate taken in the 1:1 mass ratio. The reference and counter electrode were made of lithium metal. Galvanostatic tests have been performed within the voltage range of 2.0–4.5 V at the different current rates (0.05–1C). As noticed above, the theoretical specific capacity of the compound studied, $Li||LiMn_{0.7}Fe_{0.3}PO_4$ is 170 mAh/g, therefore, 1C = 170 $mAh{\cdot}g^{-1}$.

Impedance measurements were performed using an AUTOLAB electrochemical workstation (Netherlands) by applying a harmonic perturbation signal with an amplitude of 5 mV over the frequency range from 1 MHz to 10 mHz. The obtained spectra were processed using Nova 2.1 software. To approach the equilibrium state of the electrochemical cells, each spectrum was recorded after a relaxation period of no less than 2 h. All measurements were carried out at room temperature (25 °C), with the electrochemical cells maintained in a discharged state.

The charge/discharge curves for $Li||LiMn_{0.7}Fe_{0.3}PO_4$ coin cells at 0.05C are shown in Fig. 1. These curves exhibit two pairs of well-defined plateaus at approximately 3.5 V and 4.1 V, corresponding to the redox potentials of the Fe^{2+}/Fe^{3+} and Mn^{2+}/Mn^{3+} couples, respectively, with the capacity ratio of these plateaus being about 7/3, which is consistent with the Mn/Fe ratio in the raw material. The specific capacity of the coin cells with different binders varies slightly, ranging from 137 to 141 $mAh \cdot g^{-1}$, which agrees with the manufacturer's data sheet for the electrode material. At the same time, a lower specific capacity is observed during the initial cycles for the coin cells containing the NV-1A binder. As a tentative explanation and in accordance with Ref. [19], this effect is attributed to the aqueous processing technique, which promotes metal leaching, leading to the formation of Li_3PO_4 particles on the electrode surface. Although this layer improves the overall stability, it also reduces the specific capacity during the early stages of cycling.

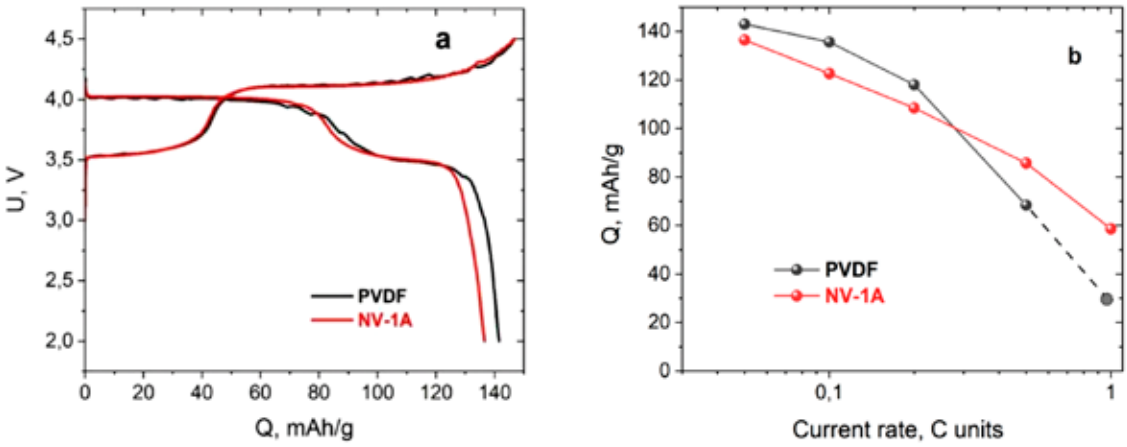

Fig. 1. Charge/discharge curves of the LMFP on the 1st cycle t 0.05C (a) and the change in specific capacity depending on the density of the discharge current (in "C" units) (b).

The coulombic efficiency obtained in the first cycle for $Li||LiMn_{0.7}Fe_{0.3}PO_4$ coin cells is 96.0 % (± 0.5 %) for the PVDF binder and 94 % (± 0.5 %) for NV-1A, respectively, and increases to 99.5 % (± 0.1 %) in the third cycle. An increase in the charge/discharge current density leads to a regular decrease in specific capacity (Fig. 1b). However, the decrease in specific capacity for $Li||LiMn_{0.7}Fe_{0.3}PO_4$ with the PVDF binder is more pronounced. Thus, at 0.5C, the

specific capacity of Li||$LiMn_{0.7}Fe_{0.3}PO_4$ is 68 and 85 mAh·g^{-1} for coin cells with PVDF and NV-1A binders, respectively. This sharp drop in specific capacity when using PVDF is attributed to the higher cell resistance associated with this binder material, as discussed below.

The cycling performance of Li||$LiMn_{0.7}Fe_{0.3}PO_4$ coin cells fabricated with the two types of binders is shown in Fig. 2. Cycles 1–35 reflect the variation in specific capacity upon cycling at different current densities (from 0.05C to 0.5C). Reference cycles 36–40 demonstrate the capacity retention after power tests, reaching 98% and 93% for the PVDF and NV 1A binders, respectively. Although cells with NV 1A exhibited lower initial capacity, their degradation at 0.1C (cycles 41–90) was only 0.1% per cycle versus 0.45% for PVDF. Although cells with NV 1A exhibited lower initial capacity, their degradation at 0.1C (cycles 41–90) was only 0.1% per cycle versus 0.45% for PVDF. Consequently, the capacity retention of the NV 1A-based cells exceeds that of PVDF-based cells after 75 cycles (Fig. 2). To explain this behavior, cell degradation was evaluated by electrochemical impedance spectroscopy (EIS).

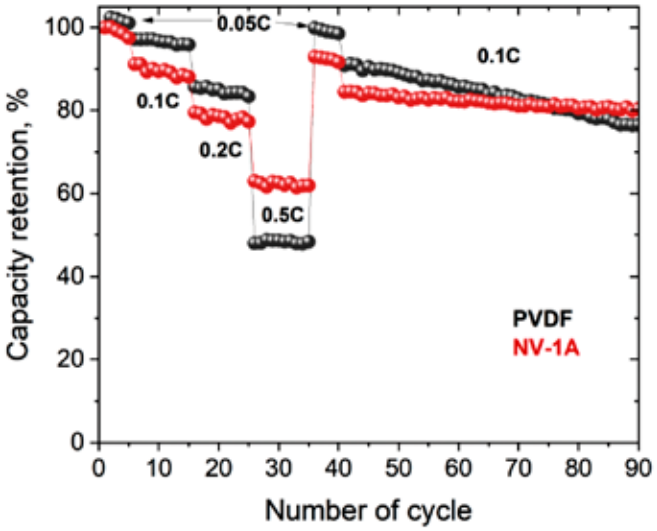

Fig. 2. Capacity retention of the LMFP electrodes upon cycling.

The change in impedance spectra upon cycling of Li||$LiMn_{0.7}Fe_{0.3}PO_4$ coin cells in 2032 case is shown in Fig. 3. Nyquist diagrams present a noticeable transformation of the impedance spectra from a "freshly assembled" sample to a sample "after 40 cycles". Namely, one semicircle of the spectrum, observed in the frequency range from $1 \cdot 10^5$ to 20 Hz and responsible for the process of charge transfer across the "electrode-electrolyte" interface, transforms into two clearly visible semicircles after 40 cycles. The first lies in the frequency range of $1 \cdot 10^5 \div 30$ Hz, while the second ranges from 30 to 0.5 Hz. These semicircles can be correlated with charge transfer processes across the "electrode-electrolyte" interface, where the first semicircle corresponds to charge transfer through the SEI formed on lithium metal

(R1). This is evidenced by the coincidence of the frequency range in the Bode diagrams of the impedance spectra of a coin cell with varying degrees of degradation, accompanied by a slight shift of the maximum to the low-frequency region with an increase in the number of cycles. The second semicircle, observed in the frequency range from 30 to 0.5 Hz, is absent in the freshly assembled element.

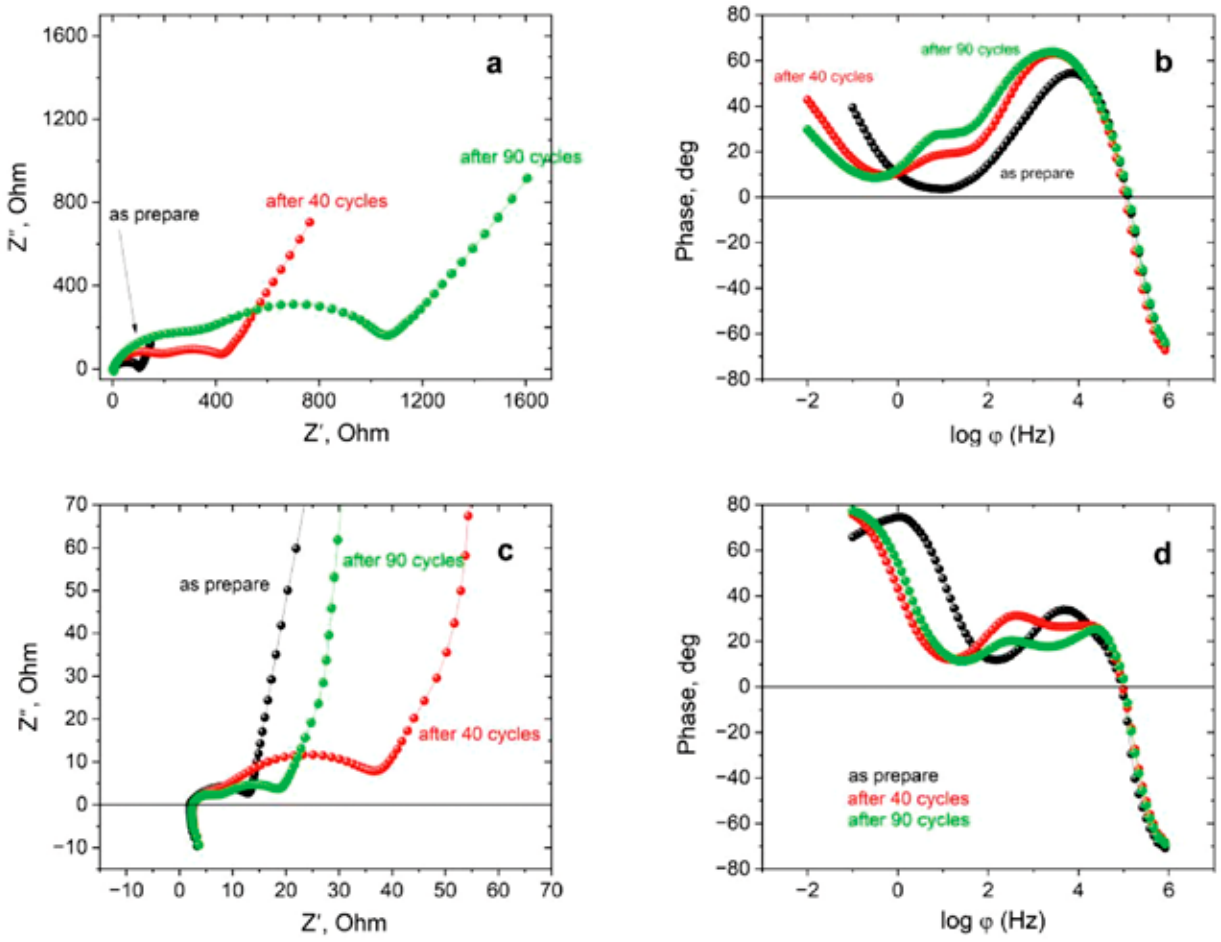

Fig. 3. Nyquist diagrams, and Bode diagrams with varying degrees of degradation of the coin cell, cathode composition: 90% - LMFP+ 5% - super P + 5% binder (a,b – PVDF; c,d – NV-1A).

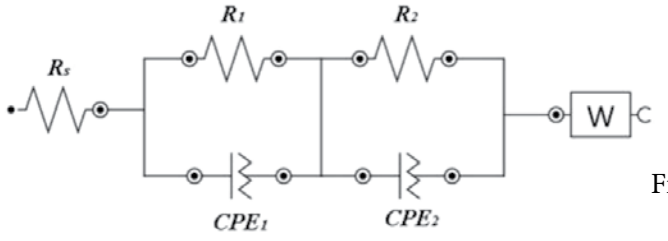

Fig. 4. An equivalent circuit used in processing impedance spectra.

The appearance and transformation of this arc can be observed upon cycling of the coin cell, which is characteristic of the formation of a high-resistance SEI film (probably due to the formation of a poorly conductive layer on the surface of the electrodes consisting of products of the interaction of manganese ions with an electrolyte at high potentials, for example MnF_2, $MnCO_3$ [20] on the surface of the cathode material *(R2)*. In addition, the frequency of the maximum of the second f_{max} arc is in the typical range for cathodic charge transfer in lithium-ion batteries (usually 0.001–0.5 kHz). SEI on lithium usually manifests itself at higher frequencies (1–100 kHz), which is observed in the impedance spectra [21, 22].

The equivalent circuit used in the fitting of impedance spectra is shown in Fig. 4. The R_s parameter in the equivalent circuit corresponds to the resistance of the electrolyte in the separator pores and is determined in the frequency range of 1–0.1 MHz. It should be noted that the R_s values exhibit non-monotonic dynamics upon cycling, which is typical for lithium-ion cells and is associated with a combination of physicochemical processes (changes in wettability, contact resistances, temperature fluctuations, etc.). However, the absolute changes in R_s do not exceed 0.7 Ω, which amounts to less than 1% of the total cell resistance R_{ct} at low frequencies and does not significantly affect the regularities discussed in this work. Table 1 lists the calculated parameters of the constituent elements and their variation upon cycling of the LMFP cells.

Table 1.

EIS data for the electrodes with different types of binders.

Binder	Parameter							
	State of the coin cell	$R_{s,}$ Ohm	$R_{1,}$ Ohm	$R_{2,}$ Ohm	$R_{ct,}$ Ohm	f_{max}, Hz	$C_{dl,}$ μF	$A_{active,}$ cm²
PVDF	as prepare	3.20	-	-	103.50	-	-	-
	after 40 cycles	2.90	226	368	492	4	108.00	5.41
	after 90 cycles	3.50	480	936	1164	4	32.50	2.13
NV-1A	as prepare	2.01	-	-	12.57	-	-	-
	after 40 cycles	2.71	6.85	34.19	38.49	150	27.56	1.38
	after 90 cycles	2.47	5.00	15.28	19.25	150	69.40	3.47

* – The measurement error of the equivalent circuit parameters does not exceed 5%.

To estimate the double-layer capacitance (C_{dl}) and to calculate the electrochemically active surface area (A_{act}) of the electrode, the parameters of the low-frequency arc were employed. This arc corresponds to the charge transfer process through the solid electrolyte interphase (SEI) formed on the cathode material. The resistance *R2* and the maximum frequency f_{max} of this arc allow C_{dl} to be calculated using the formula for a parallel RC circuit, under the assumption that the low-frequency arc is not significantly distorted by diffusion:

$$C_{dl} = \frac{1}{2\pi f_{\max} R2}, \quad (1)$$

where f_{max} is the frequency at the apex of the arc, corresponding to the maximum of the imaginary component -Z" on the charge-transfer semicircle.

The electrochemically active surface area A_{act} is related to the double-layer capacitance by the following expression:

$$A_{act} = \frac{C_{dl}}{S_{sp}}, \quad (2)$$

where S_{sp} is the specific double-layer capacitance per unit of true surface area. For smooth electrodes, this value typically lies in the range of 10 - 40 μF/cm^2, and may be slightly higher for porous or rough surfaces.

In the present work, a value of S_{sp}=20 μF/cm^2 was adopted for calculations. This is a commonly accepted reference value for flat surfaces and is widely used in the literature (e.g., Moriguchi et al. [23] reported a value of 20 ± 2 μF/cm^2 for ideal carbon surfaces). Similar values have been reported by other authors. For instance, Hang Shi estimated the specific double-layer capacitance on the micropore surface to be approximately 15–20 μF cm^{-2} [24]. This assumption was introduced for comparative purposes to assess the relative changes in the electrochemically accessible surface area upon cycling within the same series of experiments. It should be emphasized that the obtained A_{act} values do not represent the absolute true surface area, but rather provide an effective electrochemically active surface area within the framework of a smooth-electrode model.

The calculated A_{act} values reliably reflect the relative changes in the surface area available for electrochemical processes during cycling. For the PVDF-based electrodes, a decrease in A_{act} from 5.41 cm² (after 40 cycles) to 2.13 cm² (after 90 cycles) was observed. This trend correlates well with the increase in charge-transfer resistance R2 and the corresponding drop in capacity retention from 98% to 76%, respectively. These findings suggest progressive surface passivation and loss of active sites due to the formation of a blocking interfacial layer.

In contrast, for the PAA-based electrodes, a decrease and subsequent stabilization of the charge-transfer resistance *R2* was observed, along with a steady increase in A_{act}. This indicates an expansion of the electrochemically active surface area, which may be attributed to continuous electrolyte infiltration and/or the development of microcracks without loss of electrical contact between particles. The capacity retention for the PAA-based samples was found to be 92% and 80% after 40 and 90 cycles, respectively, further confirming the superior performance of this binder compared to PVDF.

CONCLUSIONS.

A comparative study of the $LiMn_{0.7}Fe_{0.3}PO_4$ cathode material with two types of polymer binders (conventional PVDF and water-soluble NV-1A (PAA-based)) reveals significant differences in their electrochemical behavior upon cycling.

1. The charge transfer resistance (*Rct*) for the electrodes based on the NV-1A binder remains practically unchanged upon cycling (from 12.6 Ω as prepared to 15.3 Ω after 90 cycles), whereas for the PVDF-based electrodes a nearly 10-fold increase in Rct*Rct* is observed (from 103.5 Ω to 936 Ω after 90 cycles). This indicates a substantially higher stability of the electrode/electrolyte interface when using the water-soluble binder.

2. The use of the NV-1A binder results in higher specific capacity of the material at C/2

and higher rates, as well as lower capacity loss upon cycling, compared to the standard PVDF binder. These observations are consistent with the impedance data and confirm the better electrochemical performance of the PAA-based system.

3. The calculated effective electrochemically active surface area (A_{act}) for the NV-1A-based electrodes shows an increasing trend upon cycling (from 1.38 cm^2 after 40 cycles to 3.47 cm^2 after 90 cycles), whereas for the PVDF-based electrodes a decrease is observed (from 5.41 to 2.13 cm^2). The observed increase in A_{act} for the PAA-based system may be tentatively attributed to progressive electrolyte infiltration and/or the development of microcracks without loss of electrical contact between particles, which could lead to additional surface availability for electrochemical reactions. However, direct evidence for this hypothesis is not available within the scope of the present work, and the obtained A_{act} values should be considered as relative estimates rather than absolute surface areas. In contrast, the decrease in A_{act} for the PVDF-based electrodes is consistent with gradual blocking of the electrode surface by the accumulation of electrolyte decomposition products and/or manganese dissolution products (e.g., MnF_2, $MnCO_3$), leading to reduced availability of active sites for lithium-ion insertion and ultimately resulting in capacity decay upon prolonged cycling.

Overall, the water-soluble binder NV-1A demonstrates clear advantages over the conventional PVDF binder in terms of interfacial stability and capacity retention, making it a promising candidate for high-performance LMFP cathodes. Further studies, including post-cycling surface analysis (e.g., SEM, XPS, or BET), are required to clarify the mechanism of the observed increase in the electrochemically active surface area.

ACKNOWLEDGMENTS.

We appreciate the international collaboration with Zhejiang Casnovo New Materials Co., Ltd (China) and the opportunity to conduct a series of studies using its laboratory facilities.

AUTHORS' CONTRIBUTION:

O.V. Potapenko: investigation, methodology, datacuration, visualization, writing – original draft.
H.V. Potapenko: supervision, conceptualization, methodology, writing review & editing.
V.O. Oliinyk: writing – original draft, visualization, data curation, writing review & editing.
V.A. Sirosh: investigation, data curation, visualization.
Changji Zhou: investigation, data curation.
Chee Sien Wong: data curation.
Changbo Yu: investigation, data curation.
Chenchun Zhang: data curation, visualization.

All authors have read the results of the study and approved the final version of the manuscript.

CONFLICT OF INTEREST. The authors declare no conflict of interest.

FUNDING. This work was carried out with the support of the National Academy of Sciences of Ukraine as part of a research project commissioned by the Chemistry Department of the National Academy of Sciences of Ukraine titled "Modification of materials obtained from the recycling of lithium iron phosphate batteries in order to improve their energy characteristics", registration number 0126U001632.

ВПЛИВ ПРИРОДИ ЗВ'ЯЗУВАЧА НА ЕЛЕКТРОХІМІЧНІ ВЛАСТИВОСТІ КАТОДНОГО МАТЕРІАЛУ $LiMn_{0.7}Fe_{0.3}PO_4$

О. В. Потапенко[1], Г. В. Потапенко[1,2], В. О. Олійник[1], В. А. Сірош[1], С. Тичина[1], Чанцзі Чжоу[2], Чі Сянь Вонг[2,3], Чанбо Юй[2], Ченьчунь Чжан[2]

[1] Інститут загальної та неорганічної хімії ім. В.І. Вернадського НАН України, просп. Академіка Палладіна, 32/34, Київ 03142, Україна;
[2] Компанія «Чжецзян Касново Нью Матеріалс» (Zhejiang Casnovo New Materials Co., Ltd.), вул. Чжунке, 1, вулиця Чжаньмао, район Путуо, м. Чжоушань, провінція Чжецзян, Китай;
[3] Факультет нафтохімічної інженерії та довкілля, Чжецзянський океанічний університет, Південна вулиця Хайда, 1, вулиця Лінчен, район Дінхай, м. Чжоушань, провінція Чжецзян, Китай
e-mail: 1978hiking@gmail.com

Дослідження присвячено електрохімічному порівнянню макетів ґудзикового типу $Li||LiMn_{0.7}Fe_{0.3}PO_4$ з використанням двох різних полімерів: PVDF та водорозчинного зв'язувача NV-1A. Криві заряджання/розряджання, отримані за струму 0.05 C, демонструють два чітко виражені плато приблизно при 3.5 В та 4.1 В, які відповідають окисно-відновним парам Fe^{2+}/Fe^{3+} та Mn^{2+}/Mn^{3+} відповідно. Співвідношення ємностей цих плато становить близько 7:3, що відповідає співвідношенню Mn/Fe у вихідному матеріалі. Питома ємність макетів ґудзикового типу з різними матеріалами-зв'язувачами знаходиться в межах 137–141 мАгод·г$^{-1}$ та узгоджується з паспортними характеристиками матеріалу. Однак на перших циклах макети ґудзикового типу з NV-1A демонструють дещо нижчу питому ємність. Це пов'язано з можливим утворенням частинок Li_3PO_4 на поверхні електрода, що призводить до зменшення питомої ємності на початкових циклах, але покращує загальну стабільність при тривалому циклюванні. Кулонівська ефективність першого циклу становить 96.0 % для PVDF та 94 ± 0,5 % для NV-1A, збільшуючись до 99.5 ± 0.1 % при подальшому циклуванні для обох систем. Збільшення густини струму заряду/розряду призводить до зменшення питомої ємності $LiMn_{0.7}Fe_{0.3}PO_4$, проте це зменшення є більш вираженим для PVDF: при 0.5 C ємність становить 68 мАгод·г$^{-1}$ для PVDF та 85 мАгод·г$^{-1}$ для NV-1A. Випробування циклічної стабільності показали, що, незважаючи на нижчу початкову ємність макетів ґудзикового типу на основі NV-1A, швидкість деградації їхньої ємності становить лише 0.1 % за цикл при 0.1 C, тоді як для PVDF цей показник дорівнює 0.45 %. У результаті після 75 циклів макетів ґудзикового типу із NV-1A демонструють кращу схоронність заряду. Отримані результати додатково обговорюються з точки зору механізмів деградації електродів у процесі циклування.

Ключові слова: полімерний зв'язувач, водорозчинний зв'язувач, літій-манган-залізо-фосфат, гальваностатичне циклування, електрохімічна імпедансна спектроскопія, збереження ємності.

REFERENCES

[1] Sciatti F., Tamburrano P., Distaso E., Amirante R., Radogna A.V., Morciano A., Grassi G. A comprehensive overview of lithium-ion batteries for electric vehicles: Materials, performance, safety, recycling, and emerging technologies. *J. Energy Storage*. 2026. **144**: 119694–119726. https://doi.org/10.1016/j.est.2026.119694.

[2] Xu C., Dai Q., Gaines L., Hu M., Tukker A., Steubing B. Future material demand for automotive lithium-based batteries. *Commun. Mater*. 2020. **1**: 99. https://doi.org/10.1038/s43246-020-00095-x.

[3] Manfo T.A., Laaksonen H. A Comparative study of the modified high voltage olivine-phosphate $LiMPO_4$ (M = Fe, Mn, Co, Ni) as promising cathode materials for next-generation rechargeable batteries. *J. Energy Storage*. 2026. **160**: 121797–121823. https://doi.org/10.1016/j.est.2026.121797.

[4] Dorri M., Nekahi A., Ahmed S., Dawkins J.I.G., Guimaraes T.M.S., Kumar M.R.A., Zaghib K. Exploring sustainable lithium iron phosphate cathodes for Li-ion batteries: From mine to precursor and cathode production. *J. Power Sources*. 2025. **656**: 238041–238061. https://doi.org/10.1016/j.jpowsour.2025.238041.

[5] Hirayama Y., Oikawa M., Yokoyama A., Kegami J., Ishida H., Ogami T. Electrochemical performance of spherical $LiMn_{0.7}Fe_{0.3}PO_4$ cathode materials for lithium-ion batteries. *Muki Mater*. 2025. **32** (Suppl.): P. 38–46. https://doi.org/10.11451/mukimate.25.Suppl.07.

[6] Wen Z. et al. Research progress in lithium manganese iron phosphate cathode material modification. Energy Storage Sci. Technol. 2024. https://doi.org/10.19799/j.cnki.2095-4239.2023.0771.

[7] Huang S., Lin W., Li L. et al. Pathway for high-energy density $LiMnFePO_4$ cathodes. *Prog. Nat. Sci.: Mater. Int*. 2023. **33** (1): 126–131. https://doi.org/10.1016/j.pnsc.2023.01.003.

[8] Zeng Y., Wang X., Li X. et al. Sustainable $LiFePO_4$ and $LiMn_xFe_{1-x}PO4$ (x = 0.1–1) cathode materials for lithium-ion batteries: A systematic review from mine to chassis. *Mater. Sci. Eng. R: Rep*. 2024. **159**: 100797. https://doi.org/10.1016/j.mser.2024.100797.

[9] Yang L., Deng W., Xu W. et al. Unlocking the full potential of $LiMn_{1-x}Fe_xPO_4$: Advances in synthesis, modification, and future directions for high-energy cathode materials. *Mater. Today Energy*. 2025. **52**: 101965. https://doi.org/10.1016/j.mtener.2025.101965.

[10] Ajayi S.O., Dolla T.H., Makgwane P.R. et al. A review of aqueous-based binders used for cathode fabrication in lithium-ion batteries. *RSC Sustain*. 2026. **4**: 1160–1179. https://doi.org/10.1039/D5SU00849B.

[11] Yoon J., Lee J., Kim H. et al. Polymeric binder design for sustainable lithium-ion battery chemistry. Polymers. 2024. 16: 254. https://doi.org/10.3390/polym16020254.

[12] Rolandi A.C., de Meatza I., Casado N., Forsyth M., Mecerreyes D., Pozo-Gonzalo C. Unlocking sustainable power: Advances in aqueous processing and water-soluble binders for NMC cathodes in high-voltage Li-ion batteries. *RSC Sustain*. 2024. **2**: 2125–2149. https://doi.org/10.1039/D4SU00098F.

[13] Crosby A.J., Hageman M., Duncan A. Controlling polymer adhesion with "pancakes". *Langmuir*. 2005. **21**: 11738–11743. https://doi.org/10.1021/la051721k.

[14] Li J., Sun J., Shi H., Liu J. Water-based binder and cathode slurry for lithium-ion battery as well as preparation methods for water-based binder and cathode slurry: Pat. CN104789160A China. № CN201510161982.7; filed 08.04.2015; publ. 22.07.2015.

[15] Yuca N., Zhao H., Song X. et al. A systematic

investigation of polymer binder flexibility on the electrode performance for lithium-ion batteries. *ACS Appl. Mater. Interfaces*. 2014. **6**(19): 17411–17418. https://doi.org/10.1021/am504736y.

[16] Aoki S., Han Z.J., Yamagiwa K., Yabuuchi N. et al. Acrylic acid-based copolymers as functional binder for silicon/graphite composite electrode in lithium-ion batteries. *J. Electrochem. Soc*. 2015. **162** (12): A2245–A2249. https://doi.org/10.1149/2.0171512jes.

[17] Hu H., Zhang L., Jin S., Hu W., Jiang N., Xu X., Zhou J. Water-soluble binder, lithium-ion battery cathode paste prepared by using water-soluble binder, preparation methods and coating methods thereof: Pat. CN104293239A China. № CN201410521837.0; filed 30.09.2014; publ. 21.01.2015.

[18] Zhang Y., Liu X. et al. Beyond binding: A review on binders in high-voltage transition metal oxide cathode of lithium-ion battery. *J. Energy Storage*. 2024. **97**: 112816. https://doi.org/10.1016/j.est.2024.112816.

[19] Akhilash M., Salini P.S., John B., Sujatha S., Mercy T.D. A comparative study of aqueous- and nonaqueous-processed Li-rich $Li_{1.5}Ni_{0.25}Mn_{0.75}O_{2.5}$ cathodes for advanced lithium-ion cells. *RSC Sustain*. 2024. **2**: 416–424. https://doi.org/10.1039/D3SU00168G.

[20] Wohlfahrt-Mehrens M., Vogler C., Garche J. Aging mechanisms of lithium cathode materials. *J. Power Sources*. 2004. **127**: 58–64. https://doi.org/10.1016/j.jpowsour.2003.09.034.

[21] Schmidt J.P., Chrobak T., Ender M., Illig J., Klotz D., Ivers-Tiffée E. Studies on $LiFePO_4$ as cathode material using impedance spectroscopy. *J. Power Sources*. 2011. **196**: 5342–5348. https://doi.org/10.1016/j.jpowsour.2010.09.121.

[22] Qiu X.-Y., Zhuang Q.-C., Zhang Q.-Q., Cao R., Qiang Y.-H., Ying P.-Z., Sun S.-G. Investigation of layered $LiNi_{1/3}Co_{1/3}Mn_{1/3}O_2$ cathode of lithium ion battery by electrochemical impedance spectroscopy. *J. Electroanal. Chem*. 2013. **688**: 393–402. https://doi.org/10.1016/j.jelechem.2012.09.027.

[23] Moriguchi I., Nakahara F., Furukawa H., Yamada H., Kudo T. Colloidal Crystal-Templated Porous Carbon as a High Performance Electrical Double-Layer Capacitor Material. *Electrochem. Solid-State Lett*. 2004. **7**(8): A221–A223. https://doi.org/10.1149/1.1756491.

[24] Shi H. Activated carbons and double layer capacitance. *Electrochim. Acta*. 1996. **41**: 1633–1639. https://doi.org/10.1016/0013-4686(95)00416-5.

Стаття надійшла: 09.04.2026.
Статтю прийнято до друку: 13.05.2026.
Статтю опубліковано: 25.06.2026.